ELSEVIER

Surface Science 511 (2002) 379–386

SURFACE SCIENCE

www.elsevier.com/locate/susc

Co on *h*-BN/Ni(1 1 1): from island to island-chain formation and Co intercalation

W. Auwärter *, M. Muntwiler, T. Greber, J. Osterwalder

Physik-Institut, Universität Zürich, Winterthurerstrasse 190, CH-8057 Zürich, Switzerland

Received 18 January 2002; accepted for publication 8 March 2002

Abstract

The growth of cobalt on a monolayer of hexagonal boron nitride on Ni(1 1 1) has been studied in a combination of scanning tunneling microscopy and X-ray photoelectron spectroscopy (XPS). A detailed picture of the growth kinetics is obtained. The Co sticking coefficient strongly decreases at high substrate temperatures. Co deposition results in two different morphologies: (i) three-dimensional clusters that grow on top of the hexagonal boron nitride (*h*-BN) film and often align themselves to form chains and (ii) islands with a more two-dimensional character, which are intercalated below the *h*-BN film dominate at higher substrate temperatures. From XPS measurements at different deposition temperatures an activation energy for intercalation of ~0.24 eV is inferred. The influence of observed defect lines in the *h*-BN overlayer on the growth kinetics is discussed.

Keywords: Scanning tunneling microscopy; X-ray photoelectron spectroscopy; Nickel; Cobalt; Clusters; Surface defects

1. Introduction

The control of interfaces is a prerequisite for continued device miniaturization down to the nanometer scale, and it is essential for the full understanding and exploitation of physical phenomena such as spin dependent electron tunneling. Atomically sharp interfaces are needed for the investigation of the physics of metal–insulator–metal (MIM) structures. Here a single layer of hexagonal boron nitride (*h*-BN) on nickel, on top of which another metal is grown, serves as a model system for an ultimately thin tunneling junction. *h*-BN is well suited for this purpose, as it is a thermally stable, chemically inert and insulating material with a band gap of about 5 eV [1]. Well defined *h*-BN films of one monolayer (ML) thickness can be grown on Ni(1 1 1) [2,3]. The resulting compact film forms a commensurate 1×1 structure with the lattice constant of Ni(1 1 1). The graphite-like sheet corrugates slightly for compensation of the small lattice mismatch (0.5%). The layer is fully aware of the C_{3v} threefold rotational symmetry of the substrate given by a closed-packed combination of *two* hexagonal Ni layers, and one particular threefold orientation develops [4,5]. This study reports on the deposition of cobalt on these almost perfect *h*-BN/Ni(1 1 1) layers: The sticking probability of Co on *h*-BN/Ni(1 1 1) is strongly temperature dependent which indicates a small activation energy difference between Co desorption and diffusion, respectively. Furthermore, two different

* Corresponding author. Fax: +41-1-635-5704.
E-mail address: williau@physik.unizh.ch (W. Auwärter).

0039-6028/02/$ - see front matter
PII: S0039-6028(02)01545-5

island growth modes and the self-assembly of island chains are observed. STM permits to distinguish them by means of their shape and adhesion and identifies defect lines in the *h*-BN layer to play a key role for the understanding of these coexisting island types: Co islands may grow on top or intercalate below the *h*-BN layer. Photoelectron spectroscopy (XPS) is used to further characterize the Co islands: from XPS measurements during Co deposition the two island types may be distinguished and the temperature dependence of XPS intensity ratios shows that the intercalation process is thermally activated.

2. Experimental

Two separate vacuum systems pumped by turbo molecular, ion and cerium getter pumps (base pressure below 5×10^{-11} mbar) and equipped with standard surface preparation tools were used for the experiments. We measured the photoemission data (XPS) in a modified VG ESCALAB 220 spectrometer [6]. Monochromatized and focussed Al Kα ($\hbar\omega = 1486.6$ eV) radiation was used to take the XP spectra. The real space images of the surface were taken by a Park Scientific Instruments [1] VPII scanning tunneling microscope, mounted in a stand-alone vacuum chamber on a home-built, vibration-isolated table. The STM images were recorded at room temperature and, unless stated otherwise, in constant-current mode with negative sample bias using electrochemically etched tungsten tips. The Ni(1 1 1) single crystal was prepared by cycles of 800 eV Ar^+ sputtering followed by exposure to 30 L O_2 at 300 K and subsequent annealing to 1000 K [7]. To grow well defined monolayers of *h*-BN the Ni(1 1 1) substrate was kept at 1070 K while dosing about 60 L of borazine ($B_3N_3H_6$). A more detailed description of the procedure is found in Refs. [3,8]. We checked the sample cleanliness and the film quality by XPS and UPS or by STM. Co and Cu were evaporated from water-cooled sources by resistively heating a tungsten filament surrounded by a metal wire (Co, Cu) of high purity (99.99%). The pressure during evaporation stayed in the mid 10^{-10} mbar range. A typical evaporation rate was about 3.5 ML/h as monitored by a quartz microbalance and calibrated by STM or XPS. During evaporation, we kept the sample at a constant temperature referred to as deposition temperature.

[1] Now: ThermoMicroscopes, 1171 Borregas Avenue, Sunnyvale, CA 94089.

3. Results and discussion

3.1. STM

STM measurements of *h*-BN monolayers on Ni(1 1 1) show large flat terraces of about 500 Å average size separated mainly by monoatomic steps of the same height as those on clean Ni(1 1 1) [3]. In Fig. 1 the two different island types which are formed after Co evaporation on such films can be seen. Deposition of Co at room temperature results in the surface structure shown in Fig. 1(a): small, several layer high clusters with an apparent diameter of about 3 nm are visible. This corresponds to the Volmer–Weber growth mode, where the bond energy between two adatoms is larger than the bond energy between adatom and substrate. In well resolved images the clusters exhibit a hexagonal outline not generated by the tip (top inset). The determination of the true cluster size is not straightforward since for such three-dimensional (3D) objects the tip shape induced broadening has to be taken into account. One notices in Fig. 1(a) that the Co clusters are not uniformly distributed on the terraces nor aligned along steps, but tend to form chains. The magnetism of Co can be ruled out as the cause for this behaviour since the same experiment with nonmagnetic Cu also leads to chain formation (not shown). Therefore the alignment has to be induced by the substrate. The chain orientations correspond to the close-packed $\langle \bar{1}\,1\,0 \rangle$ directions of the surface, as indicated in the bottom inset of Fig. 1(a).

The completely different morphology of the islands shown in Fig. 1(b) is the result of evaporating Co at a deposition temperature of 450 K at a comparable flux: larger, flat islands of triangular shape and a monoatomic step height dominate the

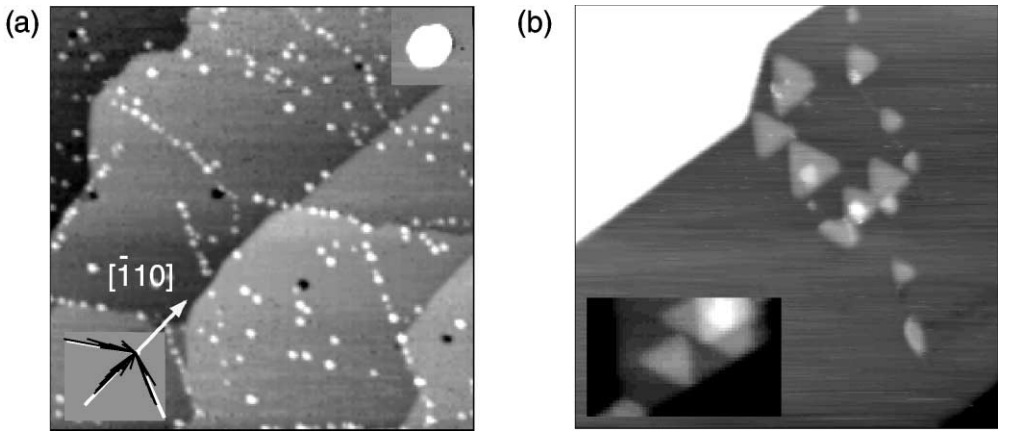

Fig. 1. STM pictures of Co evaporated on *h*-BN/Ni(1 1 1). (a) Co evaporation at RT results in 3D clusters. The clusters of hexagonal shape (top inset) often align in chains along close-packed substrate directions as indicated in the bottom inset: black lines correspond to chain directions, white lines represent the crystal directions. (1050×1050 Å^2, $I_t = 0.5$ nA, $V_t = -0.8$ V). (b) At higher evaporation temperatures (450 K) islands of a more 2D character form. They grow layer by layer at higher Co exposures (inset) (1000×1000 Å^2, $I_t = 1$ nA, $V_t = 0.06$ V).

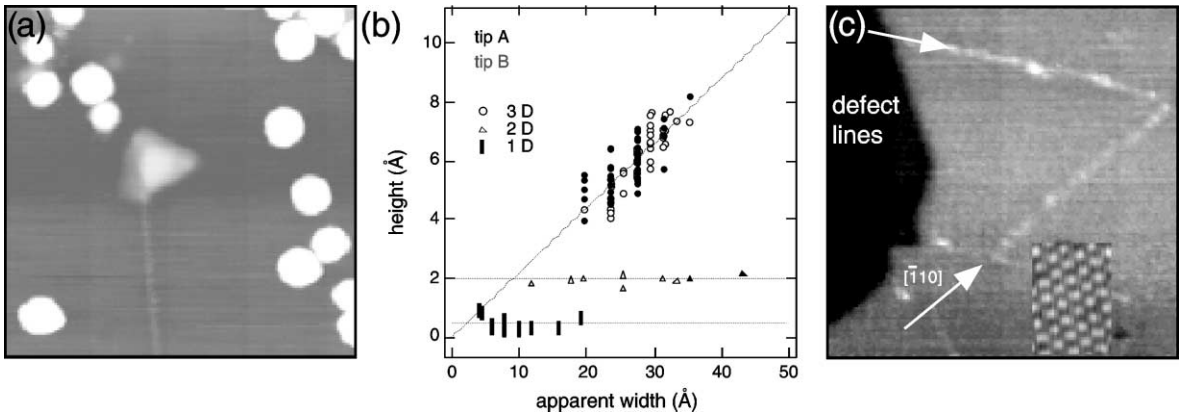

Fig. 2. (a) Coexistence of the two island types after Co evaporation at 300 K. The triangular shaped 2D island is attached to a defect line in the *h*-BN monolayer (270×270 Å^2, $I_t = 1$ nA, $V_t = 0.5$ V). (b) Height-versus-width plot of the 3D clusters, 2D islands and 1D defect lines taken from two STM images measured with different tips. The height values in this graph are not calibrated. (c) Defect lines on a bare *h*-BN monolayer before Co evaporation. The close-packed crystal directions are indicated by arrows and visualized in the inset showing atomic resolution. (425×425 Å^2, $I_t = 0.5$ nA, $V_t = 1$ V).

images. We will refer to them as "two-dimensional" (2D), although the island character is not strictly 2D: they grow layer by layer at higher Co exposures (see inset Fig. 1(b)). Annealing of 3D clusters up to 600 K for 1 h does not yield the 2D-type islands shown in Fig. 1(b). This indicates that the kinetics are important for the understanding of the two competing island types. It turns out that the 3D clusters grow on top of the *h*-BN layer, while the flat islands are intercalated between the *h*-BN monolayer and the Ni substrate.

Arguments are given in Fig. 2: In Fig. 2(a) it is shown that the two island types can coexist on the surface after Co deposition at one temperature (300 K). Note that the flat island is connected to a line in the STM image. Such lines are found also

on bare *h*-BN monolayers (Fig. 2(c)). They coincide with the close-packed directions of the substrate ($\langle\bar{1}10\rangle$, chain directions in Fig. 1) and appear in high-resolution STM images as elevations much smaller than monoatomic steps ($\sim$0.5 Å). The height-versus-width plot in Fig. 2(b) illustrates that the two island types and the lines found in STM images like Fig. 2(a) show a well distinguishable behaviour. The data points were extracted from two STM images taken with different tips. While the 3D cluster height increases linearly with the apparent width, the 2D islands height is constant and corresponds to that of a monoatomic substrate step. The much smaller height of the defect lines is independent of the apparent width. These line defects could originate from the growth mode of the *h*-BN film. When *h*-BN patches join to form a compact layer there is not enough catalytically active Ni(1 1 1) area available for the decomposition of a borazine ring. These imperfections have the same directions as the chains and may also trigger the island-chain formation mentioned above. Taking a closer look at the 2D islands created preferentially by Co deposition at elevated temperature, one can see that the *h*-BN related defect lines may cross these islands without loss in sharpness as seen in Fig. 3(a). This is a first indication, that the flat island species is intercalated below the *h*-BN.

A second clue comes from manipulation experiments: By adjusting the scan parameters (i.e. reducing the tunneling resistance) and using the STM tip as a "hoover" it is possible to clear *h*-BN regions completely from 3D clusters. We also managed to remove single islands in a controlled way (Fig. 3(c)). At a critical tip–sample separation, the whole cluster jumps to the STM-tip, leaving behind a weakly corrugated region (footprint). This results in a retraction of the tip, often combined with a change in resolution. The footprints provide a possibility to estimate the "true" diameter of the contact area of the cluster with the substrate: a hemispherical cluster shape approximation based on the measured height describes the cluster shape more realistically than the apparent cross section in the STM scans and gives a lower limit of the cluster size. From this the number of Co atoms in a 3D cluster as shown in Fig. 1 is estimated to be $N \geqslant 100$.

This controlled manipulation of clusters may be used for the tailoring of structures at surfaces (see Fig. 3(c)) or it may be a way to coat STM tips. Cluster removal by STM was demonstrated on various systems; see for example [9–11]. The important point here is that only the 3D clusters are affected by this manipulation procedure; the 2D islands may not be removed (Fig. 3(b)). This means that the 2D islands are bound more strongly to the surface, which is consistent with the picture

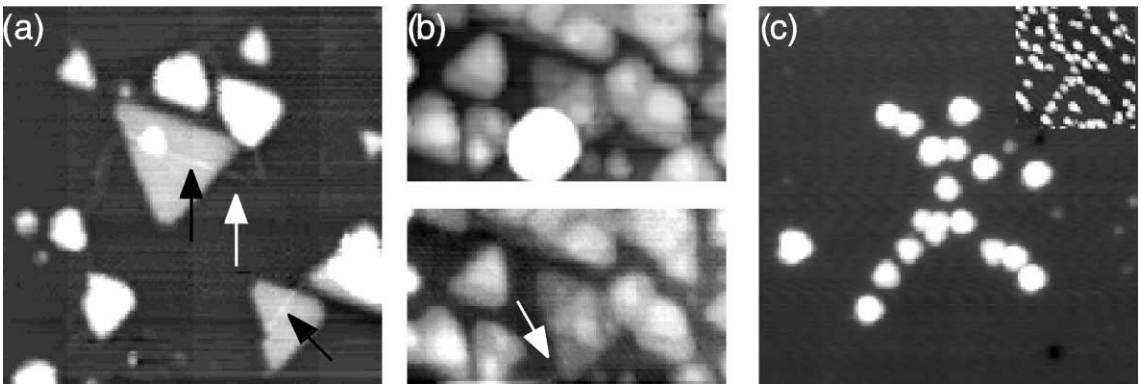

Fig. 3. (a) Defect lines are crossing 2D islands. (430 × 430 Å^2, $I_t = 2$ nA, $V_t = -0.1$ V) (b, c) Manipulation of Co clusters by the STM tip. (b) shows that 3D Co clusters are removed by the tip operating at a small tunneling resistance, while the layered 2D islands are not affected (625 × 345 Å^2, $I_t = 0.5$ nA, $V_t = -1$ V). (c) gives an example of the controlled removal of clusters by the tip resulting in a defined structure (soccer player). The initial cluster configuration is displayed in the inset. (900 × 900 Å^2, $I_t = 0.25$ nA, $V_t = -0.5$ V).

of the 3D clusters sitting on and the 2D islands lying below the *h*-BN monolayer.

Fig. 3(b) suggests the presence of stacking faults in the interface: the triangular shape of the 2D islands indicates that one of the two structurally distinguishable close-packed step edges is favoured energetically or has a higher growth speed [12]. Assuming that the same step edge is preferred independently of the island height, one can distinguish hcp from fcc stacking sequences: hcp stacking results in triangles changing orientation from layer to layer, while fcc stacking leads to triangles pointing in the same direction on all layers. Consequently, Fig. 3(b) shows that both fcc and hcp stacking sequences are present (compare also Fig. 1(b)).

3.2. XPS

In combination with the information from the STM measurements, the analysis of core level photoelectron intensities of substrate and adsorbate peaks yields the Co coverage, and further information on the growth modes and kinetics may be obtained. As the Al Kα photoemission cross section of B 1s is about four times smaller than that of N 1s [13], we focussed in these measurements on the N 1s ($E_B = 398$ eV) and the Co 3p ($E_B = 60$ eV) core level peaks. The Ni 3p ($E_B = 67$ eV) signal was used as a reference. The binding energies E_B are given relative to the Fermi energy. Our experimental setup allows to measure XPS signals during Co deposition at a desired substrate temperature while the Co flux is monitored by a quartz-microbalance. Before and after every experiment the microbalance reading was translated into a Co evaporation rate (ML/h) by comparing it to the increase of the Co signal on a Ag polycrystal, where the sticking probability is assumed to be unity. The amount of Co on Ag was determined by comparing the Co 2p signal with the Ag 3d peak integral from the clean surface scaled with the appropriate photoelectron cross sections and the photoelectron mean free paths at the given energies. From this it was possible to measure Co uptake curves as a function of sample temperature at well defined Co evaporation rates and to compare them to the XPS signals from the substrate taken in the same run. The temperature dependence of the sticking coefficient s of Co on *h*-BN as well as the intensity ratio of N:Co was determined by this procedure (see Fig. 4).

The sticking probability s of Co on the *h*-BN monolayer is discussed first. Fig. 4(a) displays the amount of Co on the sample as a function of Co exposure and temperature. 1 ML corresponds to 1.86×10^{15} atoms/cm^2. The sticking coefficients s are obtained directly from the initial slopes of the Co uptake curves. Obviously, the sticking probability decreases strongly with increasing temperature. This temperature dependence of the sticking coefficient s may be characterized with a precursor model described by Kisliuk [14]: An incoming atom first adsorbs on the surface in a weak attractive potential. From this precursor state it may pass into a more strongly bound (chemisorbed) state, i.e. in our case attach to a cluster, or desorb. The population of the precursor state is given by the incoming flux of atoms minus the amount of atoms desorbing or passing into the chemisorbed state. The branching ratio for attachment to a cluster or desorption is a ratio of two Boltzmann factors containing the activation energy for diffusion E_d into the chemisorbed state and the binding energy E_P of the precursor state. Both of them are weighted with a prefactor (k_d and k_P, respectively).

Within the Kisliuk model the sticking coefficient is the increase in population of the chemisorbed state per incoming flux. This gives two rate equations describing the dynamical equilibrium, which yield the relationship between s, the energy difference $\Delta E = E_P - E_d$ and the ratio k_d/k_P:

$$\frac{s}{1-s} = \frac{k_d}{k_P} \exp\left(\frac{\Delta E}{k_B T}\right) \tag{1}$$

In Fig. 4(b) $\ln(s/1-s)$ is plotted versus $1/T$ and thus ΔE and k_d/k_P may be extracted. For $T \geqslant 295$ K, we get $\Delta E = 140 \pm 30$ meV and $k_d/k_P = 1/200$. These two parameters give important insight into the kinetics of the formation of the Co nanostructures. The value $k_d : k_P \ll 1$ justifies the assignment of E_d as the activation energy for diffusion across many lattice sites until a Co cluster is found. It has to be noted that the present data set allows no statement on a possible temperature dependence of k_d/k_P which is e.g. imposed

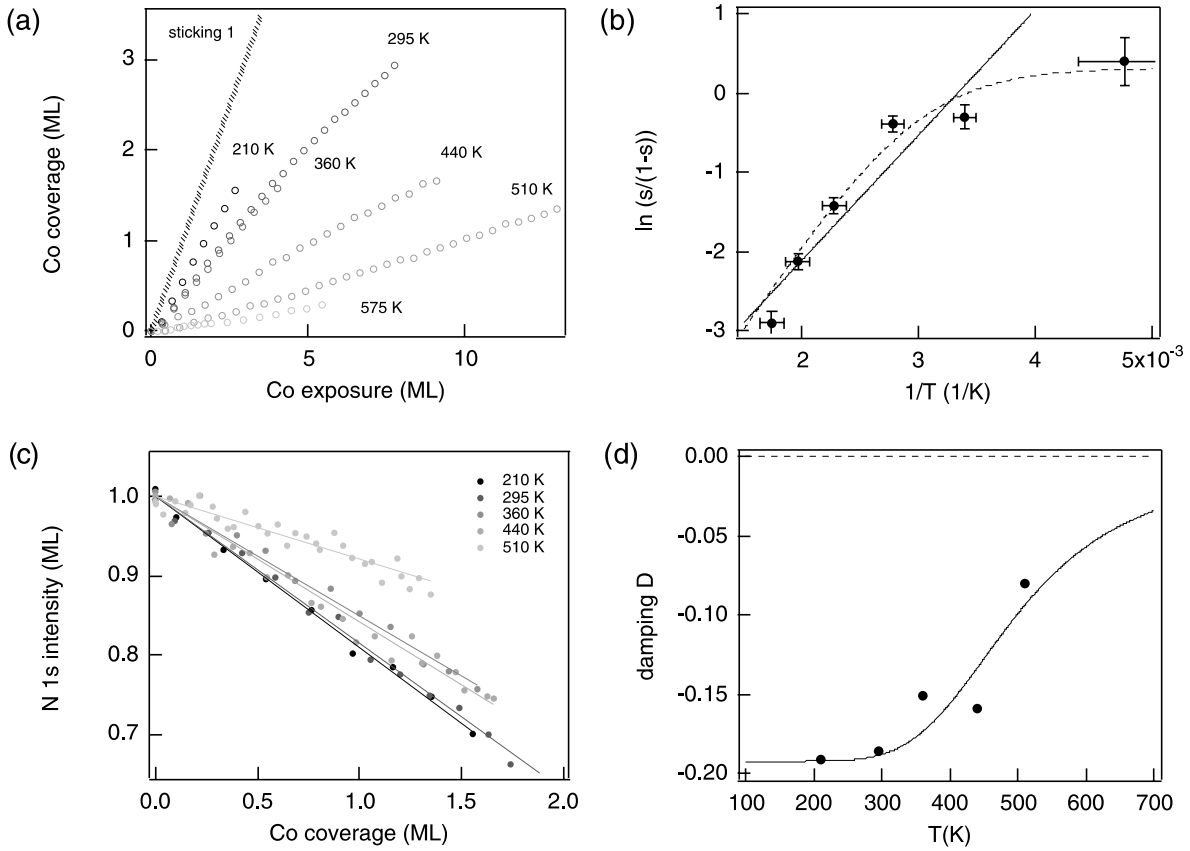

Fig. 4. XPS intensity analysis of the growth kinetics of Co on *h*-BN/Ni(1 1 1). (a) Co coverage as a function of Co exposure at various temperatures. (b) Logarithm of the sticking probability s over $1-s$ for Co on *h*-BN as a function of inverse temperature. The fit results based on the Kisliuk model (solid line) and on an extension of this model (dashed line) are discussed in the text. (c, d) Damping of the N 1s XPS signal during Co evaporation as a function of evaporation temperature. (c) shows the N 1s intensity (normalised to 1 ML) as a function of the Co coverage. The slope of the N 1s signal at a given temperature, named damping D, is displayed in (d). As it is already seen in (c), the N signal from the *h*-BN film is damped more strongly by the Co at lower temperatures than at higher ones. The damping D is assumed to saturate towards higher temperatures, but such data points were not measured because of the decreasing sticking probability of Co. Information on the displayed fit function is given in the text. The dashed line $D(T) = 0$ indicates that the N 1s intensities do not alter after heating bare *h*-BN/Ni(1 1 1) to over 900 K and demonstrates the high temperature stability.

by a temperature dependent island density. The small, though positive value of ΔE on the other hand indicates that the binding energy of a single Co atom on *h*-BN/Ni(1 1 1) must be rather small compared to the binding energy of a single Co atom on Ni(1 1 1).

The data points in Fig. 4(b) do not lie on a straight line as one would expect if the Kisliuk model describes the adsorption kinetics completely. In particular the sticking does not approach unity with decreasing substrate temperature as it is expected from the model for $\Delta E \gg k_B T$.

There are two reasons for the deviation: First there might be a systematic error in the determination of the sticking coefficient, since we assume the same homogeneous film morphology for Co on polycrystalline Ag and for Co on *h*-BN/Ni(1 1 1). In the latter case Co grows in clusters that are several layers high, which results in damped XPS signals from the buried layers. If we assume clusters with a height of three layers (see Fig. 2(b)) and layer by layer growth on Ag, we have to rescale the *s*-values from Fig. 4(a) with a factor of $\gamma = \Lambda/(\Lambda - 3d)$, where Λ is the electron mean free

path of Co 2p photoelectrons and d the layer spacing. Furthermore the influence of the two different island morphologies would have to be taken into account. This is, however, a higher order effect. A second deviation from the Kisliuk model could be direct backscattering of hot Co atoms from the evaporator upon an attempt to populate the precursor state. If we extend the model accordingly by introducing a probability factor α for substrate temperature independent direct backscattering and rescale the sticking coefficient from Fig. 4(a) by a morphology factor γ of 1.17 we get the dashed line in Fig. 4(b). It bases on the formula (compare Eq. (1))

$$\frac{s\gamma}{1-\alpha-s\gamma} = \frac{k_d}{k_P}\exp\left(\frac{\Delta E}{k_B T}\right) \tag{2}$$

The dashed line is given by the fit parameters $\Delta E = 190$ meV, $k_d/k_P = 1/300$ and a direct backscattering probability α of $\sim$30%. Compared to the initial model the value of ΔE is somewhat higher. The two values for ΔE give an estimate for a realistic error.

In a second set of experiments the behaviour of the N 1s intensity as a function of Co coverage was determined, in order to get information on the degree of capping of the h-BN by Co. Since the sticking probability of Co on h-BN drops by about one order of magnitude in a temperature region from 200 to 600 K (compare Fig. 4(a)), we are experimentally limited by the need to deposit large amounts of Co on h-BN at elevated temperatures. However, it can be seen in Fig. 4(c) that the ratio between the N 1s and Co 3p peak integrals changes significantly within the accessible temperature window. While the N 1s signal from the h-BN film decreases strongly with increasing Co coverage around RT, the signal is less damped at higher temperatures. As the island geometry has only a small influence on this ratio, we conjecture that the fraction of Co situated underneath the h-BN monolayer increases with increasing temperature: The h-BN is floating like a "carpet" on the flat Co islands and on the Ni(1 1 1) substrate and acts as a surfactant.

This point is worked out more quantitatively: From Fig. 4(c) we extract for each temperature a quantity D which describes the damping of the N 1s signal with increasing Co coverage. These dampings $D(T)$ correspond to the slopes of the attenuation curves in Fig. 4(c). The values of D are determined in the linear regime up to a Co coverage of about 1.5 ML for five temperatures and are displayed in Fig. 4(d). Up to these coverages, the clusters are still far from forming a closed film. The solid line is a fit to the data points based on a simple kinetic model. The damping D is described by the following function:

$$D = \frac{\Delta I_N}{\Delta I_{Co}} = \frac{\Delta I_N}{\Delta I_{Co3D} + \Delta I_{Co2D}} \tag{3}$$

where ΔI_{Co3D} and ΔI_{Co2D} are the Co 3p intensities from 3D and 2D Co islands, which accumulated under a given Co exposure. The maximum intensity loss of N 1s where the h-BN film is covered by 3D clusters is described by $\alpha = \Delta I_N/\Delta I_{Co3D}$. No N damping is assumed for the growth of 2D islands (i.e. $\Delta I_N/\Delta I_{Co2D} = 0$). With these assumptions, D can be written as follows:

$$D = \alpha\frac{\Delta I_{Co3D}}{\Delta I_{Co3D} + \Delta I_{Co2D}} \tag{4}$$

To model the temperature dependence of D, we assume that the growth of 2D islands is thermally activated and controlled by the energy E_A^{2D}: $\Delta I_{Co2D} = k_2\exp(-E_A^{2D}/k_B T)$, while ΔI_{Co3D} has a constant value k_3 independent of temperature (i.e. $E_A^{3D} \ll E_A^{2D}$). The branching ratio $\beta = k_3/k_2$ is a relevant kinetic factor that describes the efficiency of building 3D clusters or 2D islands, respectively.

In order to reduce the free parameters for the model, we kept α at a fixed value of -0.192, which corresponds to the base line of the damping curve in Fig. 4(d). The value depends, to a first order approximation, on the cross section ratio for photoionization of the N 1s and Co 3p levels, on the h-BN layer thickness and on the mean free paths Λ of the photoelectrons. Calculating α from these given quantities results in a value of -0.163. This number is close to the experimental value (-0.19) and further justifies the model expressed in Eq. (4). E_A^{2D} and β are thus the only free parameters.

The fit (see Fig. 4(d)) yields an activation energy E_A^{2D} of 0.24 ± 0.1 eV for Co intercalation below the h-BN layer and a value of $1/250$ for β. This activation energy for intercalation is in the same order

of magnitude as that for Li ions in a Ti oxyfluoride film [15]. β on the other hand is much smaller than unity which may be explained by the higher probability for a Co atom to find a site for intercalation than a cluster. If these two processes were to obey the same kinetics, i.e. $\beta = 1$, this would lead to a 1:1 equilibrium of the two island types at high temperatures (i.e. $k_B T \gg E_A^{2D}$). In this case, the damping D would not tend towards zero, but saturate at $-\alpha/2$. Such an equipartition of 3D clusters and 2D islands at high temperatures is, however, inconsistent with our STM data too (see Fig. 1(b)). The defect lines as observed with STM (Fig. 2) supply an important clue for the small branching ratio β. If the defect lines which are linked with intercalated islands act as line-like traps for Co atoms, they must be, due to their one-dimensional (1D) character, much more efficient for catching Co atoms than the zero-dimensional clusters on top of *h*-BN/Ni(1 1 1).

4. Conclusions

Apart from Co cluster chain formation on *h*-BN/Ni(1 1 1), we report multiple evidence, given by different experimental techniques, for thermally activated intercalation of Co under a *h*-BN monolayer. From this it becomes evident that evaporation at low temperatures is necessary to get a MIM system of high quality. The intercalated islands are closely related to defect lines, which serve as "collectors" for Co that intercalates. Besides temperature the *h*-BN film quality, in particular the compactness of the layer, will have a crucial influence on the Co growth and intercalation behaviour.

Acknowledgements

We are grateful to D. Menzel for bringing the Kisliuk model to our attention and to H. Sachdev for the production of borazine. This work was supported by the Swiss National Science Foundation.

References

[1] A. Catellani, M. Posternak, A. Baldereschi, A.J. Freeman, Phys. Rev. B 36 (1987) 6105.
[2] A. Nagashima, N. Tejima, Y. Gamou, T. Kawai, C. Oshima, Phys. Rev. Lett. 75 (1995) 3918.
[3] W. Auwärter, T.J. Kreutz, T. Greber, J. Osterwalder, Surf. Sci. 429 (1999) 229.
[4] Y. Gamou, M. Terai, A. Nagashima, C. Oshima, Sci. Rep. RITU A 44 (1997) 211.
[5] M. Muntwiler, T. Greber, J. Osterwalder, Surf. Sci. 472 (2001) 125.
[6] T. Greber, O. Raetzo, T.J. Kreutz, P. Schwaller, W. Deichmann, E. Wetli, J. Osterwalder, Rev. Sci. Instrum. 68 (1997) 4549.
[7] T.J. Kreutz, T. Greber, P. Aebi, J. Osterwalder, Phys. Rev. B 58 (1998) 1300.
[8] A. Nagashima, N. Tejima, Y. Gamou, T. Kawai, C. Oshima, Phys. Rev. B 51 (1995) 4606.
[9] M.D. Upward, P. Moriarty, P.H. Beton, S.H. Baker, C. Binns, K. Edmonds, Appl. Phys. Lett. 70 (16) (1997) 2114.
[10] P.J. Durston, R.E. Palmer, J.P. Wilcoxon, Appl. Phys. Lett. 72 (2) (1998) 176.
[11] S.J. Chey, L. Huang, J.H. Weaver, Appl. Phys. Lett. 72 (21) (1998) 2698.
[12] P. Grütter, U.T. Dürig, Phys. Rev. B 49 (3) (1994) 2021.
[13] J.J. Yeh, I. Lindau, At. Data Nucl. Data Tables 32 (1985) 1.
[14] P. Kisliuk, J. Phys. Chem. Solids 3 (1957) 95.
[15] M.S. Mattsson, G.A. Niklasson, C.G. Granqvist, J. Appl. Phys. 80 (4) (1996).